



Data-driven design of carbon-based materials for high-performance flexible energy storage devices

Yuxuan Wang^a, Junwei Sha^a, Shan Zhu^{b,*}, Liying Ma^a, Chunlian He^a, Cheng Zhong^a, Wenbin Hu^a, Naiqin Zhao^{a,**}

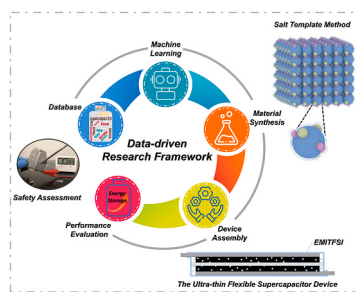
^a School of Materials Science and Engineering and Tianjin Key Laboratory of Composite and Functional Materials, Tianjin University, Tianjin, 300350, PR China

^b School of Materials Science and Engineering, Hebei University of Technology, Tianjin, 300401, PR China

HIGHLIGHTS

- A data-driven design framework for energy storage devices is proposed.
- Machine learning is used to investigate the key features of electrode materials.
- An ultra-thin flexible supercapacitor device with high safety is fabricated.

GRAPHICAL ABSTRACT



ARTICLE INFO

Keywords:

Energy storage
Flexible devices
Machine learning
Three-dimensional carbon networks
Ionic liquids

ABSTRACT

With the rise of flexible electronics, the demand for advanced power sources has grown. Developing high-performance energy storage devices requires comprehensive consideration of various factors such as electrodes, electrolytes, and service conditions. Herein, a data-driven research framework is proposed to optimize the electrode-electrolyte system in supercapacitors. With the help of machine learning, we reveal the key factors affecting the capacitance performance of carbon-based materials. According to the algorithm analysis, a kind of 3D carbon network is prepared with controlled composition and structure, which is incorporated with a high-safety ionic liquid to obtain a supercapacitor device. This device with high energy density and impressive flexibility can maintain operational stability under extreme conditions such as humidity, shock, and localized damage. Overall, this work presents a typical pipeline for accelerating the design of energy-related devices.

1. Introduction

With the rapid development of foldable electronics and wearable devices, there is an increasing demand for portable and flexible power

supplies [1–3]. Typical application scenarios of wearable electronics need to withstand high-angle bending, high-frequency shock, potential water immersion, etc. In order to cope with these demands, the applied energy storage devices have to meet the safety requirements while

* Corresponding author.

** Corresponding author.

E-mail addresses: shanzhu@hebut.edu.cn (S. Zhu), nqzhao@tju.edu.cn (N. Zhao).

ensuring high performance [4–7]. Supercapacitors have the merits of high power, long cycle life, and good thermal safety, which enable them to serve as a promising power source for wearable electronics [8–11]. However, further improvements to the supercapacitors, including enhanced energy storage ability and safety, need to be made before achieving their wider applications.

The key issue in improving the device performance is to optimize their electrode-electrolyte system. Yet, this optimization process requires a comprehensive consideration of various factors. Based on the current scientific understanding of the supercapacitors, many factors influence the capacitive properties of the electrode materials, such as surface area, pore structure, and heteroatom doped content [12–14]. Also, the electrolyte plays an essential role in the energy storage processes. For example, the electrochemical stability of the electrolyte determines the voltage window for the device's operation [15,16]. In addition to electrodes and electrolytes, the test environments, such as charge/discharge current, also affect the actual performances [17,18]. What's more, the introduction of flexible device working conditions in this system will pose a higher level of challenge. Significantly, the interaction mechanisms between the electrode and electrolyte under extreme operating conditions are still lacking sufficient research.

Because of the complex influencing factors in flexible energy storage devices, there are some ambiguities in the design of electrodes and electrolytes. When optimizing electrode materials, factors such as specific surface area and heteroatom doping need to be considered. Which factors should be given higher priority? [19,20]. Similarly, for the selection of the electrolyte, which should be considered first, energy storage ability or safety? For instance, ionic liquids have good safety, yet their high viscosity leads to limited ion diffusion efficiency and reduces the rate performance of supercapacitors [21–23]; organic electrolytes are flammable, but they can endow carbon-based materials with higher capacitance [24]. To explore each of these factors by experimental methods would be costly in terms of time and labor. To this regard, a promising solution is to shift the research from an empirical/theoretical-driven paradigm to a data-driven paradigm [25–27].

The strategy of applying machine learning (ML) to optimize experimental parameters is on the rise [28–32]. If a limited number of key influencing factors can be identified, it can certainly accelerate the design of flexible energy storage devices. Current ML is deeply involved in the preparation of energy storage devices. For example, the deep neural network was used for predicting the electrode volume change in metal-ion batteries [33]. Also, the ML-based modeling was applied to analyze the interaction between electrolyte and electrode [34,35]. Besides, At the device level, there are also many methods being developed to predict the performance or stability of batteries [36]. However, data on energy storage materials and devices are still insufficient.

Here, we propose a data-driven research framework for developing high-performance flexible supercapacitors. First, to address the complexity of the energy storage system, we utilize ML tools to filter the key factors affecting the capacitive properties of carbon-based electrodes, thereby guiding subsequent material synthesis and electrolyte selection. Based on the intelligent analysis, we select ionic liquid as electrolytes and prepared 3D carbon networks by using a controllable salt template method. Consequently, the ultra-thin flexible supercapacitor devices (FSC) are prepared using a flexible-packaging process. The comprehensive performance tests show that FSC can achieve a high energy density and stability. More importantly, the FSC can maintain working stability under extreme conditions such as needling and cutting. From data analysis to device assembly, this work presents a pipeline for data-driven design energy storage devices, which can accelerate the development of advanced applications.

2. Experimental section

2.1. Machine learning

The database was based on our previous work [37]. The specific capacitance data at different current densities were abstracted from the published paper by the WebPlotDigitizer [38], which were added to the original database. All of these data were available in Dataset S1. The algorithms of tree-based pipeline optimization technique (TPOT) was used to analyze the carbon-based supercapacitor system, and the selection of the optimized model was the gradient boosting regressor (GBR). Moreover, the TreeExplainer in the shapley additive explanations (SHAP) library was applied to calculate the Shapley value of each feature. All ML methods were conducted in Python, and the corresponding codes were available at https://github.com/Shan-Zhu/ML-SC_3DCN.

2.2. Synthesis of 3DC samples

A mixed solution was prepared, including glucose (1.8 g), NaCl (30 g), Na₂CO₃ (1 g), Na₂SiO₃ (1 g), and 120 ml of deionized water (18.2 mΩ cm⁻¹), which was stirred for 2 h at room temperature. The resulting solution was frozen at -65 °C for 24 h and freeze-dried at -70 °C in vacuum for 48 h to obtain the precursor powder. Afterward, the precursor powder was annealed to 700 °C (heating rate of 5 °C min⁻¹) for 2 h in a tube furnace under a flowing Ar atmosphere (100 sccm), followed by suction filtering and washing with deionized water to dissolve the salts. Finally, the sample was vacuum dried at 60 °C for 12 h to obtain 3DC. The same process was applied to obtain the doped sample by adding urea (1.8 g) in the initial mixed solution. The nitrogen-doped was introduced in the product during subsequent high-temperature cleavage of the nitrogen source, denoted as 3DC-N.

The 3DC-N and KOH (mass ratio = 1:3) were mixed with deionized water, followed by an evaporation step with stirred at 80 °C to a uniform mixture powder. The etching process was carried out by annealed to 800 °C for 2 h under Ar atmosphere. Next, the mixture powder was washed repeatedly with 0.1 M HCl and deionized water until the pH of the filtrate was approximately 7. The final 3DC-NE was obtained after vacuum drying at 60 °C for 12 h. The same process was applied to obtain the etched undoped sample, denoted as 3DC-E.

2.3. Materials characterization

The microstructure and morphology of samples were examined by Hitachi S4800 scanning electron microscope (SEM) at 5 kV and JEM-2100 F transmission electron microscope (TEM) at 200 kV, respectively. Raman spectra were collected with Renishaw in-Via Raman Microscope RE04 using 532 nm laser, and X-ray photoelectron spectroscopy (XPS) were recorded via Kratos Axis Supra system. Brunauer-Emmett-Teller (BET) surface areas and porosities of samples were determined by nitrogen adsorption and desorption at 77 K using a Micromeritics ASAP 2020 analyzer.

2.4. Synthesis of 3DC electrode

Firstly, all samples were mixed with Super P (SP) and poly tetra fluoroethylene (PTFE) at a mass ratio of 80: 10: 10 in ethanol and ultrasonicated for 20 min to form a homogenous mixture, respectively. The mixture was ground in a mortar to evaporate the ethanol and then rolled to obtain a carbon film. Finally, working electrodes were prepared by vacuum-drying the carbon film at 60 °C for 12 h and punching into a circle of 8 mm diameter. The active materials on each electrode were larger than 1 mg cm⁻². Two identical (by weight and size) electrodes were assembled into a test cell with a symmetry two-electrode system, using cellulose film (NKK, TF4030) as the separator and EMI-TFSI (Aladdin) as the electrolyte in an argon-filled glove box (O₂ and H₂O

levels less than 1 ppm).

2.5. Assembling of the FSC

Firstly, 3DC-NE, SP, and PTFE were mixed by the same process as above and then coated on the industrialized aluminum foil. The working electrodes were prepared by vacuum-drying the coated foil at 60 °C for 12 h and were cut to the desired size. Two identical electrodes were sandwiched with a cellulose film separator and then partially sealed in a biaxially oriented polypropylene film (BOPP) plastic package by heat lamination, leaving one side open for the electrolyte filling. The unsealed FSC was vacuum-dried at 80 °C for 12 h to remove residual moisture and complete the assembly inside the glove box. After that, the EMI-TFSI was injected into the unsealed FSC. The FSC was sealed completely by heat lamination at 100 mbar vacuum. The series and parallel connections of FSCs were assembled following the same process but using different shaped working electrodes.

2.6. Electrochemical measurements

All samples were stored for 12 h at room temperature before the measurements. The cyclic voltammetry (CV), galvanostatic charge/discharge (GCD), and electrochemical impedance spectroscopy (EIS) measurements of both electrode and device were conducted on an electrochemical workstation (IVIUM-n-STAT, Netherlands) at room temperature. EIS measurement was tested at open circuit potential within a frequency range from 100 kHz to 10 mHz by applying a 5 mV ac amplitude. The calculation processes were shown in the Supplementary data.

3. Results and discussion

3.1. Machine learning design

Fig. 1a shows the framework of this research, which starts with data collection and ends with device evaluation. For the data collection, the database of this work was upgraded from the previous database of

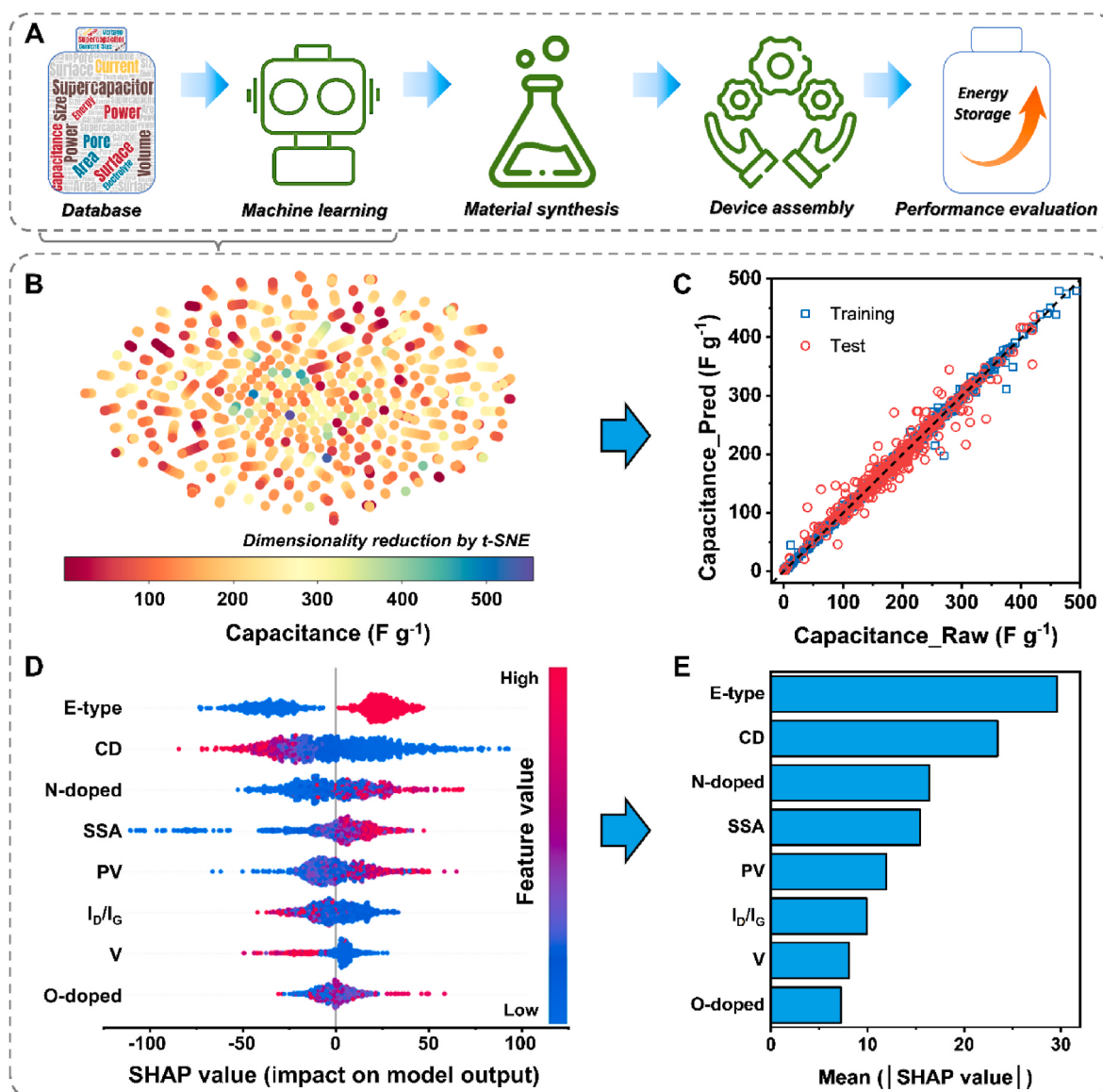


Fig. 1. ML design for flexible energy storage. (a) Schematic diagram of data-driven designing high-performance supercapacitors process. (b) The data of carbon-based supercapacitor reduced by the t-SNE algorithm. (c) Algorithm analysis results using the TPOT optimized selection algorithm. (d) SHAP analysis honeycomb diagram for each feature. (e) The average of the absolute SHAP value of each feature.

carbon-based supercapacitors [37] (Dataset S1). Specifically, we extracted the data points from the published paper and added the specific capacitance data at different current densities to the original database. The introduction of these new data could provide a more comprehensive picture of the real operating conditions of supercapacitors. In this database, three kinds of features were selected as the input: (1) the material characteristics, such as specific surface area (SSA), pore volume (PV), nitrogen-doped content (N-doped), and others; (2) the test system parameters, such as the test type (three-electrode or two-electrode, E-type), test current density (CD); (3) the electrolyte information, which mainly affects the operating voltage window (Voltage). At the output, we choose “the specific capacitance (Cap)” as the target, which directly reflects the energy storage capacity of the supercapacitor. Of course, there are some other metrics related to the performance of supercapacitors, such as cycling stability. However, there is a lack of sufficient data to integrate the cyclic stability with the properties of the electrode materials. To visualize the database, we applied the t-SNE algorithm to reduce the high-dimensional data down to 2 dimensions (Fig. 1b).

Given the database, a tree-based pipeline optimization technique (TPOT) was conducted to select the optimal ML method [39]. TPOT can automatically screen the various models and find out the most suitable one for the target database. Introducing the TOPT in data-driven material design studies not only saves time and labor, but also provides a comparable benchmark to avoid the subjectivity brought by human choice. In the calculation, we divided the database into a training set and a test set in the ratio of 8:2. By TPOT optimization, the selected model is the gradient boosting regressor (GBR), and the specific parameters are shown in Table S1. Based on the optimized ML model, we can further analyze the system of carbon-based supercapacitors (Fig. 1c). The coefficient of determination (r^2) was applied to evaluate the regression analysis results. The r^2 of the training dataset is calculated to be 0.996; for the test dataset is 0.946, approving that the selected ML model can achieve good accuracy on our database. These results have been verified by K-fold verification (Table S2). More metrics, including the mean squared error (MSE), the mean absolute error (MAE) and the root-mean-square error (RMSE), were calculated and listed in Table S3.

The SHAP algorithm was performed to open the “black box” of ML results, which can calculate the contribution of different features to the output [40]. Several trends can be observed from the SHAP outcome (Fig. 1d and e). The most significant impact on the capacitance is the test system. According to the current scientific understanding, the three-electrode test system is more responsive to the energy storage potential of the materials, while the two-electrode system is closer to the actual application environment [12]. Then, there is the current density that affects the actual operation of the devices. For the aspect of material characteristics, the most influential factors are N-doped and SSA. Surprisingly, N-doped has the greatest impact on the specific capacitance of carbon-based electrodes. The enhancement of the capacitive properties of carbon materials by the N-doping effect can be attributed to several reasons. First, the introduction of N atoms in the carbon can improve the electrical conductivity of the material [41,42]. In addition, the N-containing functional groups on the surface of carbon matrix can enhance the charge transfer at the electrolyte/electrolyte interface [43]. Also, it has been pointed out that N-doping can enhance the stability of carbon-based electrode in the high voltage window electrolytes [44].

Given the importance ranking of these features, it is reasonable to focus on the factors of SSA and N-doping content of the electrode material in the subsequent synthesis. Importantly, it should be noted that the operating voltage window (Voltage) does not have a high influence weight. The voltage window depends on the electrolyte selection. We have previously struggled with whether to pursue high storage performance or high safety in electrolyte selection. From the data point of view, since the feature of voltage window has a relatively minor influence, safety should be a high priority when selecting the electrolyte. Therefore, the ionic liquid, with high safety and electrochemical

stability, will be chosen as the electrolyte for the subsequent study.

3.2. Materials synthesis

After determining the features to focus on, we applied the salt template strategies to prepare the carbon-based electrode materials (Fig. 2a). This salt-template method is able to quantitatively control some key parameters of the carbon material. For example, we are able to achieve control of the microstructures of carbon at different scales. By exchanging different salts, it is possible to build a wide range of 3D structures from the micron scale to the nanoscale (Fig. S1). In this work, using the three kinds of salts as the mixing template, we obtained a 3D network carbon material with a hierarchical porous structure (noted as 3DC). To fit with the data analysis results, we further improved the preparation by adding urea as a nitrogen source in the precursor and introducing N-doped in the product (noted as 3DC-N). In addition, we added KOH etching to the synthesis of 3DC and 3DC-N to enhance their SSA, and the corresponding samples were named 3DC-E and 3DC-NE, respectively. All these samples present the 3D interconnected networks with hierarchical porous structures (Fig. 2b). The advantage of 3D structure can be considered from the following aspects. Firstly, the 3D structure of carbon can facilitate the formation of electron conduction pathways, which means that electrons can transport through the material more efficiently [45]. Also, due to the open character of the 3D network, this structure can ensure sufficient contact between the electrode and the electrolyte, thus enhancing the processes of ion transport [46].

The SSA and PV were measured by nitrogen isothermal adsorption and desorption tests (Fig. 2c and d), and their results were listed in Table S4. The etching process boosts the SSA from 1088.5 m²/g (3DC) to 2057.5 m²/g (3DC-E) due to the increased micropore surface area. Also, the N-doped effect can increase the external surface area of 3DC-N, because the volatilization of urea present in the precursor leaves more mesopores [47,48]. The 3D structure of 3DC-NE also remains stable after the etching process, whose SSA and PV have been improved significantly compared to 3DC. The introduction of N-containing groups enhances the hydrophilicity of the carbon matrix, which can adsorb the KOH more uniformly during the KOH impregnation process. Therefore, in the subsequent high-temperature activation, the KOH etching of 3DC-N results in the densely distributed small mesopores and the uniformly enlarged mesopores of 3DC-NE (Fig. S2).

Moreover, the elemental compositions of the obtained samples were characterized. According to the STEM and EDS of 3DC-NE (Fig. S3), the C, N, and O elements are homogeneously distributed in the network. The XPS analysis (Fig. 2e) quantifies the similar N content of 3DC-N and 3DC-EN, which are 2.51 at. % and 2.68 at. %, respectively (Table S5). In the N 1s spectra of 3DC-NE (Fig. 2f and Table S6), the peak can be divided into pyridinic N (397.94 eV), pyrrolic N (399.86 eV), graphitic N (402.36 eV), and oxidized N (405.17 eV). The N elemental analysis of 3DC-N was shown in Fig. S4. In these samples, the pyrrolic N and pyridinic N account for the majority, which are beneficial to accumulating electric charges in the electrical double layer due to the proper electron configuration and binding energy [49–51]. Besides, all 3DC samples have similar O-doped levels (Fig. 2e and Fig. S5), and the absence of Na and K elements verify the removal of salt template and KOH.

In the Raman spectra (Fig. S6), there are two peaks at D (1300–1400 cm⁻¹) and G (1584 cm⁻¹) bands, and their ratio (noted as I_D/I_G) reflects the crystallinity of carbon materials. These 3DC samples have a similar I_D/I_G ratio (0.96–1.04), proving that the defects and crystallinity are not significantly affected by the doping and etching process. Meanwhile, the broad peak (2600–2800 cm⁻¹) at the 2D band indicates the ultrathin characteristics of 3DC series samples. Overall, the key influencing factors of carbon-based electrode materials can be effectively controlled, which can lay the foundation for subsequent in-depth analysis.

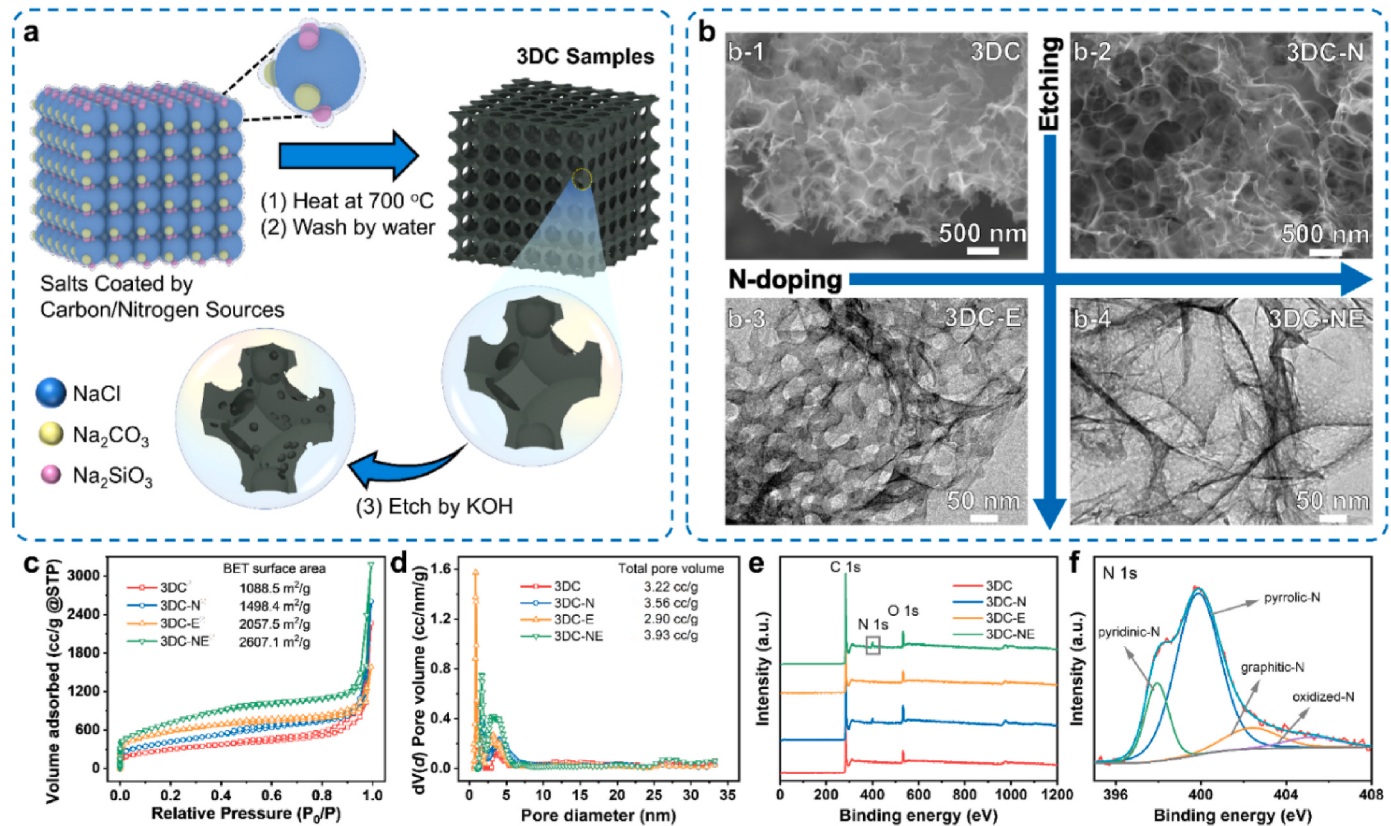


Fig. 2. Scheme for synthesis and structure of the 3DC samples. (a) Schematic diagram of material preparation process. (b) Morphology characterization: SEM image of 3DC and 3DC-N, TEM image of 3DC-E and 3DC-NE. (c) N₂ adsorption-desorption isotherm curves. (d) Pore size distribution of 3DC samples. (e) XPS spectra, and (f) the corresponding high-resolution N 1s peak analysis of 3DC-NE.

3.3. Electrochemical properties

The electrochemical properties of 3DC samples were tested by a two-electrode system using 1-ethyl-3-methylimidazolium bis(trifluoromethylsulfonyl)imide (EMI-TFSI) as the electrolyte. As shown in Fig. 3a and Fig. S7, the cyclic voltammetry (CV) curves at different scanning rates reveal their typical capacitance characteristics with presenting a rectangular-like shape in 3.2 V voltage window. Under the same test conditions, the 3DC-NE stores more charge and has good coulomb efficiency. Even at a high scanning rate of 200 mV s⁻¹ (Fig. 3b), the 3DC-NE and its companions still keep their capacitive properties due to the enhanced mass transfer ability derived from the connected network and the hierarchical pore structures [52]. In galvanostatic charge/discharge (GCD) tests (Fig. 3c), the symmetric triangle shapes of samples demonstrate their capacitance features [53]. Moreover, the specific capacitances at various current densities were calculated (Fig. S8). The 3DC-NE with both N-doped and highest SSA presents the highest specific capacitance, which can achieve 191.2 F g⁻¹ at 1 A g⁻¹, and maintain 140.2 F g⁻¹ at 50 A g⁻¹. The capacitances of 3DC-E and 3DC-N are similar at low current densities, yet 3DC-E exhibits a better rate performance at high current density, confirming the superiority of micropore surface area for fast electrolyte diffusion. For comparison, we added the capacitive performances of other N-doped carbons (Fig. S9), which were tested in similar conditions to our samples. It can be seen that 3DC-NE still exhibited superior capacitance and rate performance due to its excellent structural and compositional characteristics.

The EIS was conducted to further analyze the electrochemical properties of 3DC samples (Fig. 3d). The Nyquist plots show the typical features of the capacitor, which consists of a half circle in the high frequency area and a vertical line in the low frequency area [54]. According to Fig. 3f and Table S7, these 3DC samples exhibit similar high

frequency resistance (internal resistances, R_i). In comparison, the charge transfer resistance (R_{ct}) has a decreasing trend from 3DC, 3DC-E, 3DC-N to 3DC-NE. Additionally, the C' against Z' was plotted. As shown in Fig. 3e. The distance between the lowest and highest point represents the in-pore ionic resistances in the capacitance system, which was calculated to be 10.3, 9.8, 9.2, and 7.3 Ω for 3DC, 3DC-N, 3DC-E, and 3DC-NE, respectively. This trend reflects that 3DC-NE has the best mass transfer efficiency. Overall, the increased SSA offers a large area for ion adsorption, and the reasonable pore size distribution provides ion-access to accelerate mass transfer and facilitates electrolyte infiltration [55, 56]. Meanwhile, the N-doped enhances the electronegativity to improve the electrolyte-electrode interface for better ion adsorption and charge transfer [57, 58].

After collecting the data from the prepared samples in this study, we input these data into the trained ML model (Fig. 3g). It was found that the resulting predicted data fit the measured data relatively well. For example, the predicted capacitance of 3DC-NE is the highest among all samples and decreases with the increase of current density. It is worth noting that the predicted values for 3DC, 3DC-N, and 3DC-E are slightly higher than the measured values, while the measured values for 3DC-NE exceed the predicted values. This phenomenon can be explained by that the SSA and N-doping have a synergistic enhancement effect. Besides, we have to admit that for the 3DC materials system, there is still some error between the ML predictions and the actual measured values. These errors are due to the inadequate dimensionality of the material description and the lack of data amount in the database.

3.4. Device performances

Based on the excellent electrochemical properties of the 3DC-NE, we developed an ultra-thin flexible supercapacitor device (FSC) using 3DC-

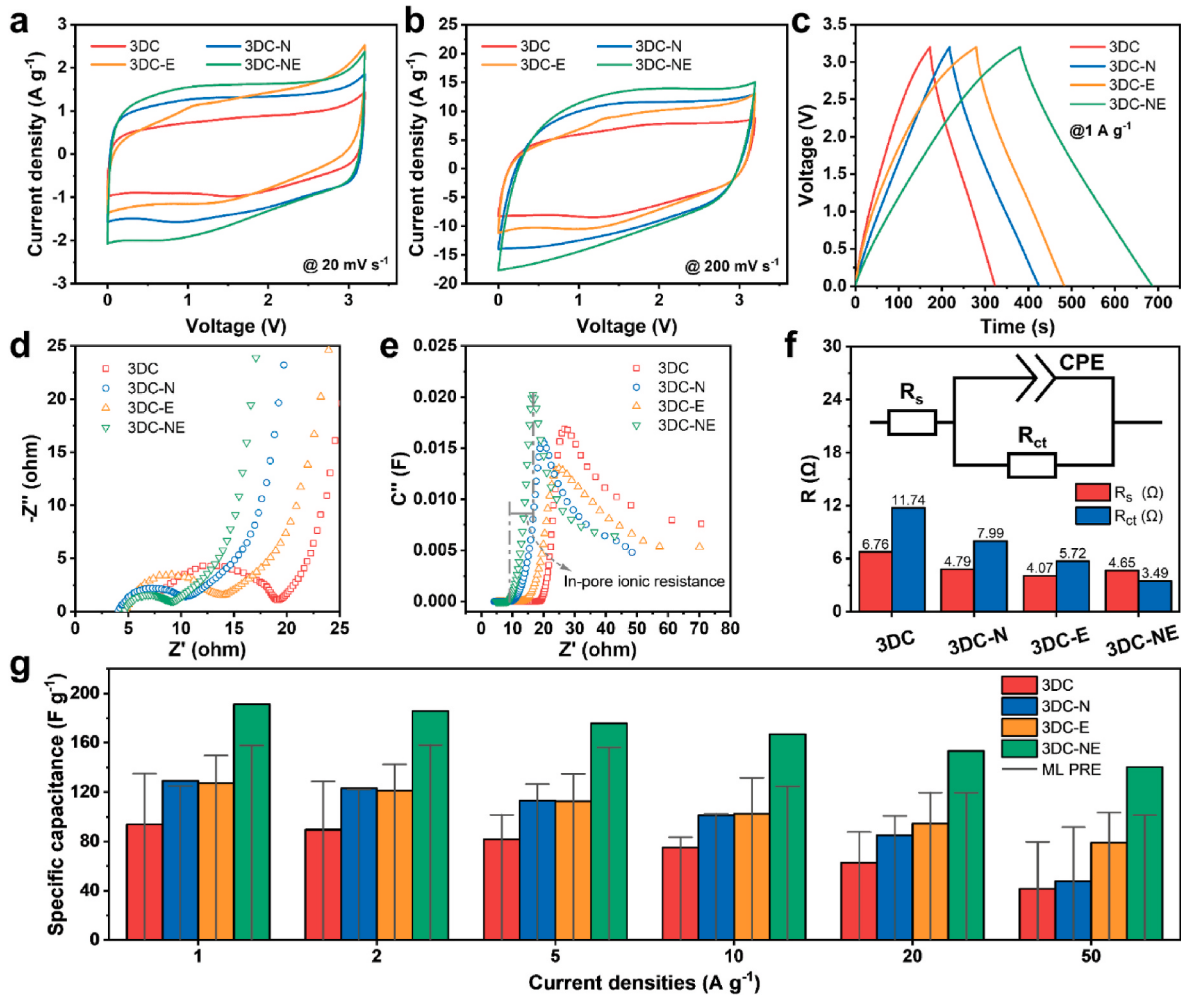


Fig. 3. Electrochemical measurement results of the 3DC samples. (a, b) CV curves at the scanning rate of 20 mV s^{-1} and 200 mV s^{-1} . (c) GCD curves at the current density of 1 A g^{-1} . (d) Nyquist plots. (e) C'' vs. Z' plot. (f) Numerical analysis of the fitted equivalent circuit. (g) Comparison of measured and ML predicted values (ML PRE) of samples.

NE as electrode material and EMI-TFSI as electrolyte. In the device design, a set of plastic packaging technology was used to ensure the good sealing and flexibility of the device (Fig. 4a). Specific details of the device assembly can be found in the experimental producers. The devices obtained by this assembly method have the advantage of controllable size and thickness. (Fig. 4b).

The CV curves of the FSC were measured under 3.0 V at different scanning rates (Fig. 4c), which shows quasi-rectangular shapes and suggests its fast charge/discharge ability. Meanwhile, the GCD results of the FSC (0.63 g) under various currents were tested (Fig. 4d), demonstrating that its calculated capacitance is 4.4 F at 10 mA . After being assembled into devices, the samples of 3DC-NE show lower capacitance. Because, to calculate the specific capacitance in the FSC, the weight of electrode material, diaphragm, electrolyte and encapsulation material were taken into account. Therefore, the resulting capacitance is numerically lower than when only the electrode material quality is considered. Besides, FSC was tested in the flexible package. The microscopic environment inside the device is still different from the ideal state, which affects the mass transfer and capacitance performance of the 3DCN-NE. To this issue, the further solutions include: (1) using lighter sealing films with thinner collectors to increase the mass share of the active materials; (2) optimizing the injection amount of electrolyte to reduce its mass ratio and ensure the performance of electrode; (3) improving the pressing process during encapsulation to enhance the contact between the electrode and the collector.

Benefiting from the optimized electrode-electrolyte system and the lightweight assembly components, the energy density and power density of the FSC (based on the weight of the entire device) are 8.7 Wh kg^{-1} at 23.8 W kg^{-1} and 5.1 Wh kg^{-1} at 238.1 W kg^{-1} , respectively (Fig. S10). Furthermore, the cycling stability of FSC at the large current was tested, indicating that the device remains about 70% of the capacitance after 2500 cycles at the current of 100 mA (Fig. S11). Besides, the series and parallel connections of FSCs can be realized to meet different output voltage requirements (Fig. S12). As shown in Fig. 4b, a series configuration FSC with a 6.0 V working voltage can power an electronic watch under the curled condition.

Consequently, we tested the performance of FSC under the extreme state. The FSC was curled around a glass rod with a diameter of 6 mm , and the obtained similar electrochemical performance proves its stability for flexible energy storage (Fig. 4e and Fig. S13). In the Nyquist plots (Fig. S14), the R_s in different states are 1.37Ω (normal) and 1.42Ω (curled), respectively (Table S8), indicating that the bending state has only a small impact on the internal resistance of the device. Reasonable material selection and assembly design ensure the light, flexibility, and stability of the device. At the same time, the liquid electrolyte provides better interfacial contact to reduce the interface resistance and further improve the device's flexibility.

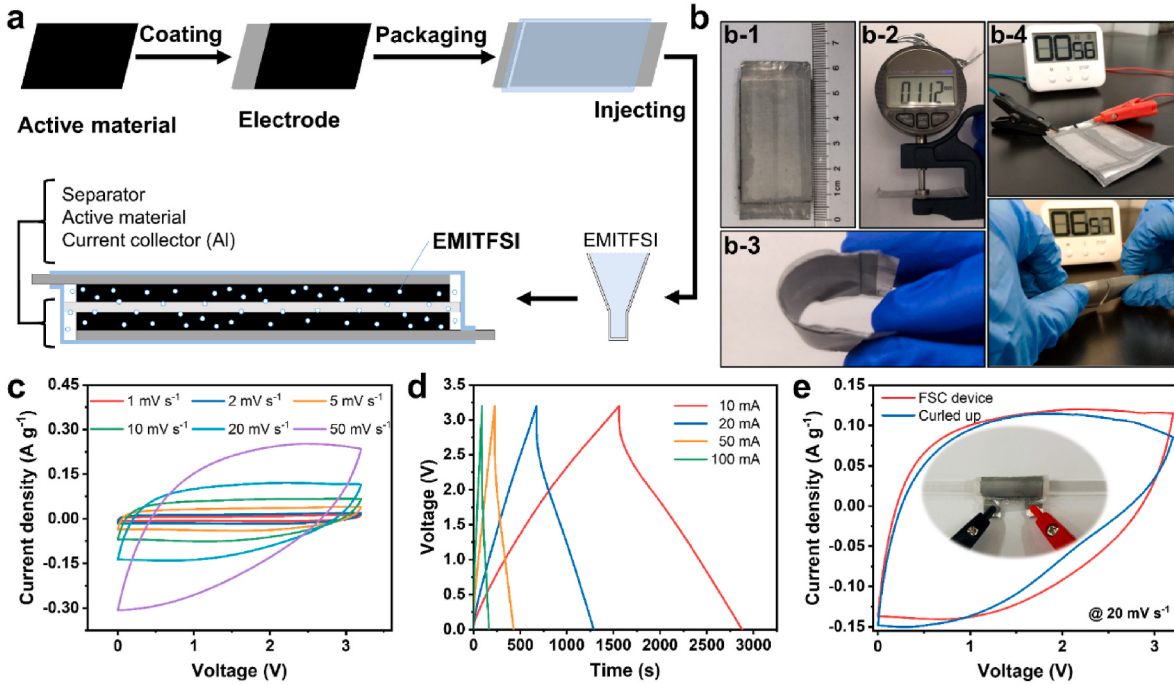


Fig. 4. Energy storage performance of the FSC. (a) Schematic diagram of FSC assembly process. (b) The length, thickness, bendability, and application under different bending states of the FSC. (c) CV curves at various scanning rates. (d) GCD curves at various currents. (e) CV curves of the FSC under different mechanical states at 20 mV s^{-1} .

3.5. Safety evaluation

Considering the unique challenges of flexible devices [59–61], we conducted a series of safety evaluation tests to simulate the extreme situations that devices may encounter in daily life. In these experiments, a series configuration of 2 FSC devices was prepared to charge the electronic clock for the demonstration (Video S1).

Supplementary video related to this article can be found at <https://doi.org/10.1016/j.jpowsour.2022.232522>). Full detailed procedures are described in Note S1.

In these experiments, the hammering test and weight loading test were performed to evaluate the mechanical stability of FSC (Fig. 5a and b), which are to simulate the crushing and shocking situation that the device will encounter in the practical situation. After each hammering, the capacitance of FSC was tested by the galvanostatic discharge at 10 mA and then recharged for the subsequent hammering. Although the capacitance of FSC is slightly reduced, 93.9% capacitance is maintained even after 10 hammer strikes. Then, several iron blocks (580 g per piece) were placed on the devices for loading testing. It is found that FSC serves well when supporting about 4000 times its own weight. All these results prove the mechanical robustness of the FSC. Besides, in a wearable electronic, there is a greater possibility of the FSC being exposed to sweat or rain. Thus, the fabricated FSC was soaked in water and tested every 2 h to check its capacitance retention (Fig. 5c). The retention fluctuates around 100% during the 20 h of soaking, demonstrating the tightness and waterproofness of packaging technology.

In addition, we performed several destructive tests on the FSC. Since the puncture can lead local short circuit and cause thermal runaway, a needle with a diameter of 1.5 mm was used to pierce the device to simulate this situation. After each puncture, the capacitance of FSC was tested by the galvanostatic discharge at 10 mA and then recharged before the next puncture. As shown in Fig. 5d, the capacitance of FSC drops significantly after the first puncture due to the vacuum disruption inside the device. However, the FSC still maintains the energy supply without electrolyte leakage and thermal runaway, and remains at over 70% capacitance retention after 10 times puncturing. Furthermore, we

conducted an extreme experiment to cut the charged FSC at random areas (Fig. 5e), and recorded the retention rate of open circuit voltage (OCP). Due to the local short circuit, the voltage of the FSC dropped as the cutting times increased. Yet, 80.1% of its initial voltage was obtained even if only half of the device is left after 10 consecutive cuttings (Fig. 5g). Additionally, this damaged FSC was soaked in water (Fig. 5f), and its power supply still retains 70.9% of the voltage after 60 min soaking. The above destructive tests were conducted on a single FSC that was charging an electronic watch, as shown in Video S1. During the test, even after the serious damage, the FSC still performs well and powers the electronic clock. Furthermore, we verified that this device can be used to power different products, such as an electroluminescent flexible display screen (Fig. S15).

The main reasons for the safety of this device are the choice of electrolyte and the optimization of the assembly process. The non-combustible ionic liquid avoids the issues of ignition and explosion; the plastic sealing ensures the flexibility of the device. What's more, we examined the interaction between the electrode and the electrolyte by adsorption tests. To this regard, the flex sheets of 3DC-NE and 3DC were prepared for the contact angle test with EMITFSI droplets (Fig. S16), and the variations of contact angle were recorded (Fig. S17). In the 3DC-NE, the initial contact angle of the droplet is 26° and decreases to 0° after 18 s. For 3DC, its initial contact angle is almost twice that of 3DC-NE (50°), the contact angle decreases more slowly, and the absorption is completed in 360s. In terms of absorption speed, 3DC-NE is nearly 18 times that of 3DC, meaning that 3DC-NE has better wettability to the ionic liquid, which allows the ionic liquid to migrate in the electrode material faster. Then, we continued to add ionic liquid (4 μL per drop) to the carbon sheets until the saturation state. The results show that 3DC-NE can absorb more electrolyte than 3DC at the same weight (Fig. S18). Besides, after absorbed ionic liquid, the carbon sheets were immersed in DI water for 60 min, then weighed after removing water by drying. It can be found that 3DC lost more than half of the ionic liquid, while the ionic liquid lost in 3DC-NE is only 7%. These experiments demonstrate that the N-doped effect and the hierarchical pore structures of 3DC-NE contribute to the strong infiltration ability to the ionic liquid. In

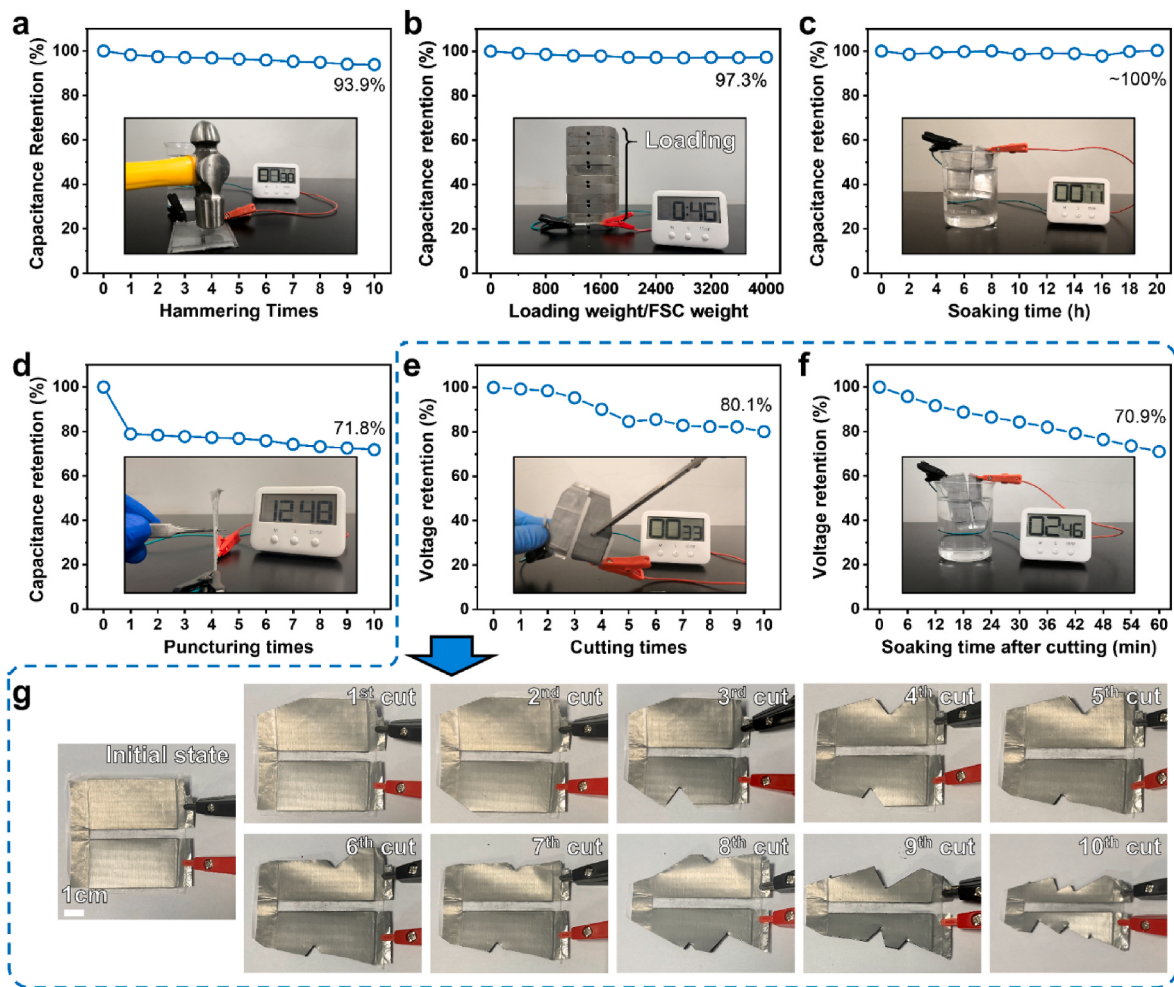


Fig. 5. Electrochemical performance of the FSC in different safety evaluation tests. (a) Hammering test. (b) Weight loading test. (c) Soaking test. (d) Puncturing test. (e) Cutting test. (f) Soaking test of cut FSC. The inset is the screenshot of Video S1 to illustrate the experiment process. (g) Digital photos of the FSC at different cutting states.

In practice usage, 3DC-NE can absorb rapidly and store stably the electrolyte to ensure the operation of the device and prevent the leakage of electrolyte in extreme or damaged conditions.

The research on this electrode-electrolyte system still has room for further improvement, which will be a multiscale synergistic task. From the atomic-level structural engineering of the materials to the assembly of the devices, all these factors need to be considered in concert. Therefore, the optimization will need to be integrated from different scales of materials and different parts of the device [62]. Moreover, this work focus on the capacitance. In future research, it is important to pay attention to a variety of indicators of the device, such as stability and rate performance. For multi-scale and multi-factor systems, the data-driven methods based on ML can play a greater role, which will further enhance the R&D efficiency of energy storage devices.

4. Conclusions

In this study, we constructed a research framework for the data-driven design of energy storage devices. Based on data collection, the ML methods were used to investigate the key features affecting the electrochemical properties of electrode materials. According to the analysis results, we selected the ionic liquid electrolyte with safety as a priority. Meanwhile, the 3DC-NE series materials were obtained by using the N-doped and surface area as major indicators to concern. Electrochemical tests showed that this electrode-electrolyte

combination can achieve high specific capacitance (191.2 F g^{-1} @ 1 A g^{-1}) with high rate performance (140.2 F g^{-1} @ 50 A g^{-1}). Moreover, a flexible device based on 3DC-NE and ionic liquid was constructed by a plastic sealing process, which can achieve high capacitance and maintain the original performance under bending and curled conditions. In particular, the FSC device can maintain good energy storage ability under extreme operating conditions such as puncture, cut, and water immersion. The reason for this remarkable safety is that the unique 3D network structure and the N-doped content of 3DC-NE can effectively adsorb and store the highly stable ionic liquid, thus ensuring the operation even after local damage. In conclusion, this research pipeline applied data analysis as a starting point to guide the subsequent material synthesis and device design, which can be extended to develop other energy storage devices.

Data statement

All ML methods were conducted in Python, and the corresponding codes were available at https://github.com/Shan-Zhu/ML-SC_3DCN. The data that support the findings of this study are available from the corresponding author upon reasonable request.

CRediT authorship contribution statement

Yuxuan Wang: Methodology, Writing – original draft, Formal

analysis, Investigation. **Junwei Sha**: Investigation, Methodology. **Shan Zhu**: Conceptualization, Software, Writing – review & editing, Supervision. **Liying Ma**: Methodology, Writing – review & editing. **Chunnian He**: Conceptualization, Formal analysis. **Cheng Zhong**: Visualization, Conceptualization. **Wenbin Hu**: Visualization, Conceptualization. **Nai-qin Zhao**: Project administration, Funding acquisition, Supervision.

Declaration of competing interest

The authors declare that they have no known competing financial interests or personal relationships that could have appeared to influence the work reported in this paper.

Data availability

Data will be made available on request.

Acknowledgements

The authors gratefully acknowledge the financial support by the National Natural Science Foundation of China [grant numbers 51771136, 51972225, and 52101020], and the Postgraduate Research and Innovation Project of Tianjin [grant number 2020YJSB144]. We also thank Ms. Y. Han and Ms. L. Ma from the National Demonstration Center for Materials Science & Engineering Education, Tianjin University for the help and kind advice on the characterization of the samples.

Appendix A. Supplementary data

Supplementary data to this article can be found online at <https://doi.org/10.1016/j.jpowsour.2022.232522>.

References

- [1] G.-H. Lee, H. Moon, H. Kim, G.H. Lee, W. Kwon, S. Yoo, D. Myung, S.H. Yun, Z. Bao, S.K. Hahn, Multifunctional materials for implantable and wearable photonic healthcare devices, *Nat. Rev. Mater.* 5 (2020) 149–165.
- [2] S. Chen, L. Qiu, H.-M. Cheng, Carbon-based fibers for advanced electrochemical energy storage devices, *Chem. Rev.* 120 (2020) 2811–2878.
- [3] G. Chen, X. Xiao, X. Zhao, T. Tat, M. Bick, J. Chen, Electronic textiles for wearable point-of-care systems, *Chem. Rev.* (2021), <https://doi.org/10.1021/acs.chemrev.1c00502>.
- [4] Y. Liu, K. He, G. Chen, W.R. Leow, X. Chen, Nature-inspired structural materials for flexible electronic devices, *Chem. Rev.* 117 (2017) 12893–12941.
- [5] H. Li, C. Han, Y. Huang, Y. Huang, M. Zhu, Z. Pei, Q. Xue, Z. Wang, Z. Liu, Z. Tang, Y. Wang, F. Kang, B. Li, C. Zhi, An extremely safe and wearable solid-state zinc ion battery based on a hierarchical structured polymer electrolyte, *Energy Environ. Sci.* 11 (2018) 941–951.
- [6] H. Li, Z. Tang, Z. Liu, C. Zhi, Evaluating flexibility and wearability of flexible energy storage devices, *Joule* 3 (2019) 613–619.
- [7] J. Wen, B. Xu, Y. Gao, M. Li, H. Fu, Wearable technologies enable high-performance textile supercapacitors with flexible, breathable and wearable characteristics for future energy storage, *Energy Storage Mater.* 37 (2021) 94–122.
- [8] A.B. Dalton, S. Collins, E. Munoz, J.M. Razal, V.H. Ebron, J.P. Ferraris, J. N. Coleman, B.G. Kim, R.H. Baughman, Super-tough carbon-nanotube fibres, *Nature* 423 (2003), 703–703.
- [9] B. Yao, S. Chandrasekaran, J. Zhang, W. Xiao, F. Qian, C. Zhu, E.B. Duoss, C. M. Spadaccini, M.A. Worsley, Y. Li, Efficient 3D printed pseudocapacitive electrodes with ultrahigh MnO₂ loading, *Joule* 3 (2019) 459–470.
- [10] E. Pomerantseva, F. Bonaccorso, X.L. Feng, Y. Cui, Y. Gogotsi, Energy storage: the future enabled by nanomaterials, *Science* 366 (2019) 969–1.
- [11] R. Kumar, E. Joanni, S. Sahoo, J.J. Shim, A. Matsuda, W.K. Tan, R.K. Singh, An overview of recent progress in nanostructured carbon-based supercapacitor electrodes: from zero to bi-dimensional materials, *Carbon* 193 (2022) 298–338.
- [12] S. Zhang, N. Pan, Supercapacitors performance evaluation, *Adv. Energy Mater.* 5 (2015), 1401401.
- [13] S. Zhu, N. Zhao, J. Li, X. Deng, J. Sha, C. He, Hard-template synthesis of three-dimensional interconnected carbon networks: rational design, hybridization and energy-related applications, *Nano Today* 29 (2019), 100796.
- [14] M. Liu, X. Li, C. Shao, C. Han, Y. Liu, X. Li, X. Ma, F. Chen, Y. Liu, Synchronous-ultrahigh conductive-reactive N-atoms doping strategy of carbon nanofibers networks for high-performance flexible energy storage, *Energy Storage Mater.* 44 (2022) 250–262.
- [15] L. Manjakkal, A. Pullanchiyodan, N. Yogeswaran, E.S. Hosseini, R. Dahiya, A wearable supercapacitor based on conductive PEDOT:PSS-coated cloth and a sweat electrolyte, *Adv. Mater.* 32 (2020), 1907254.
- [16] C. Choi, K. Robert, G. Whang, P. Roussel, C. Lethien, B. Dunn, Photopatternable hydroxide ion electrolyte for solid-state micro-supercapacitors, *Joule* 5 (2021) 2466–2478.
- [17] C. Zhong, Y. Deng, W. Hu, J. Qiao, L. Zhang, J. Zhang, A review of electrolyte materials and compositions for electrochemical supercapacitors, *Chem. Soc. Rev.* 44 (2015) 7484–7539.
- [18] C. Gao, J. Huang, Y. Xiao, G. Zhang, C. Dai, Z. Li, Y. Zhao, L. Jiang, L. Qu, A seamlessly integrated device of micro-supercapacitor and wireless charging with ultrahigh energy density and capacitance, *Nat. Commun.* 12 (2021) 2647.
- [19] M. Yu, X. Feng, Thin-film electrode-based supercapacitors, *Joule* 3 (2019) 338–360.
- [20] X.L. Shi, W.Y. Chen, T. Zhang, J. Zou, Z.G. Chen, Fiber-based thermoelectrics for solid, portable, and wearable electronics, *Energy Environ. Sci.* 14 (2021) 729–764.
- [21] D.R. MacFarlane, M. Forsyth, P.C. Howlett, M. Kar, S. Passerini, J.M. Pringle, H. Ohno, M. Watamabe, F. Yan, W.J. Zheng, S.G. Zhang, J. Zhang, Ionic liquids and their solid-state analogues as materials for energy generation and storage, *Nat. Rev. Mater.* 1 (2016), 15005.
- [22] X.H. Wang, M. Salari, D.E. Jiang, J.C. Varela, B. Anasori, D.J. Wesołowski, S. Dai, M.W. Grinstaff, Y. Gogotsi, Electrode material–ionic liquid coupling for electrochemical energy storage, *Nat. Rev. Mater.* 5 (2020) 787–808.
- [23] J. Feng, Y. Wang, Y. Xu, Y. Sun, Y. Tang, X. Yan, Ion regulation of ionic liquid electrolytes for supercapacitors, *Energy Environ. Sci.* 14 (2021) 2859–2882.
- [24] G. Lee, J.W. Kim, H. Park, J.Y. Lee, H. Lee, C. Song, S.W. Jin, K. Keum, C.H. Lee, J. S. Ha, Skin-like, dynamically stretchable, planar supercapacitors with buckled carbon nanotube/Mn-Mo mixed oxide electrodes and air-stable organic electrolyte, *ACS Nano* 13 (2019) 855–866.
- [25] A. Chen, X. Zhang, Z. Zhou, Machine learning: accelerating materials development for energy storage and conversion, *InfoMat* 2 (2020) 553–576.
- [26] J. Li, K. Lim, H. Yang, Z. Ren, S. Raghavan, P.-Y. Chen, T. Buonassisi, X. Wang, AI applications through the whole life cycle of material discovery, *Matter* 3 (2020) 393–432.
- [27] S. Zhu, C. He, N. Zhao, J. Sha, Data-driven analysis on thermal effects and temperature changes of lithium-ion battery, *J. Power Sources* 482 (2021), 228983.
- [28] D.P. Finegan, S.J. Cooper, Battery safety: data-driven prediction of failure, *Joule* 3 (2019) 2599–2601.
- [29] V. Tshiroyan, J. Dagdelen, L. Weston, A. Dunn, Z. Rong, O. Kononova, K.A. Persson, G. Ceder, A. Jain, Unsupervised word embeddings capture latent knowledge from materials science literature, *Nature* 571 (2019) 95–98.
- [30] M. Zhong, K. Tran, Y. Min, C. Wang, Z. Wang, C.-T. Dinh, P. De Luna, Z. Yu, A. S. Rasouli, P. Brodersen, S. Sun, O. Ozernyy, C.-S. Tan, M. Askarka, F. Che, M. Liu, A. Seifitokaldani, Y. Pang, S.-C. Lo, A. Ip, Z. Ullissi, E.H. Sargent, Accelerated discovery of CO₂ electrocatalysts using active machine learning, *Nature* 581 (2020) 178–183.
- [31] D.P. Finegan, J.E. Zhu, X.N. Feng, M. Keyser, M. Ulmefors, W. Li, M.Z. Bazant, S. J. Cooper, The application of data-driven methods and physics-based learning for improving battery safety, *Joule* 5 (2021) 316–329.
- [32] A. Zheng, Y. Wang, F. Zhang, C. He, S. Zhu, N. Zhao, Data-driven design and controllable synthesis of Pt/carbon electrocatalysts for H₂ evolution, *iScience* 24 (2021), 103430.
- [33] I.A. Moses, R.P. Joshi, B. Ozdemir, N. Kumar, J. Eickholt, V. Barone, Machine learning screening of metal-ion battery electrode materials, *ACS Appl. Mater. Interfaces* 13 (2021) 53355–53362.
- [34] T. Gao, W. Lu, Physical model and machine learning enabled electrolyte channel design for fast charging, *J. Electrochem. Soc.* 167 (2020), 110519.
- [35] J.F. Whitacre, J. Mitchell, A. Dave, W. Wu, S. Burke, V. Viswanathan, An autonomous electrochemical test stand for machine learning informed electrolyte optimization, *J. Electrochem. Soc.* 166 (2019) A4181.
- [36] M.F. Ng, J. Zhao, Q. Yan, G.J. Conduit, Z.W. Seh, Predicting the state of charge and health of batteries using data-driven machine learning, *Nat. Mach. Intell.* 2 (2020) 161–170.
- [37] S. Zhu, J. Li, L. Ma, C. He, E. Liu, F. He, C. Shi, N. Zhao, Artificial neural network enabled capacitance prediction for carbon-based supercapacitors, *Mater. Lett.* 233 (2018) 294–297.
- [38] A. Rohatgi, WebPlotDigitizer v4.6 (Version 4.6), Pacifica, September 16, 2022, <http://automeris.io/WebPlotDigitizer>.
- [39] T.T. Le, W. Fu, J.H. Moore, Scaling tree-based automated machine learning to biomedical big data with a feature set selector, *Bioinformatics* 36 (2020) 250–256.
- [40] S.M. Lundberg, G. Erion, H. Chen, A. DeGrave, J.M. Prutkin, B. Nair, R. Katz, J. Himmelfarb, N. Bansal, S.I. Lee, From local explanations to global understanding with explainable AI for trees, *Nat. Mach. Intell.* 2 (2020) 56–67.
- [41] J. Zhao, H. Lai, Z. Lyu, Y. Jiang, K. Xie, X. Wang, Q. Wu, L. Yang, Z. Jin, Y. Ma, J. Liu, Z. Hu, Hydrophilic hierarchical nitrogen-doped carbon nanocages for ultrahigh supercapacitive performance, *Adv. Mater.* 27 (2015) 3541–3545.
- [42] Y. Deng, Y. Xie, K. Zou, X. Ji, Review on recent advances in nitrogen-doped carbons: preparations and applications in supercapacitors, *J. Mater. Chem. 4* (2016) 1144–1173.
- [43] J.K. Ewert, D. Weingarth, C. Denner, M. Friedrich, M. Zeiger, A. Schreiber, N. Jäckel, V. Presser, R. Kempe, Enhanced capacitance of nitrogen-doped hierarchically porous carbide-derived carbon in matched ionic liquids, *J. Mater. Chem. 3* (2015) 18906–18912.
- [44] M.J. Mostazo-López, J. Krummacher, A. Balducci, E. Morallón, D. Cazorla-Amorós, Electrochemical performance of N-doped superporous activated carbons in ionic liquid-based electrolytes, *Electrochim. Acta* 368 (2021), 137590.
- [45] P. Chang, J. Zheng, Y. Cen, F. Yang, X. Li, Q. Xie, J. Dong, 3D hierarchical porous carbon from fulvic acid biomass for high energy density supercapacitor with high withstanding voltage, *J. Power Sources* 533 (2022), 231413.

- [46] Y. Wang, Y. Zeng, J. Zhu, C. Yang, H. Huang, X. Chen, R. Wang, P. Yan, S. Wei, M. Liu, D. Zhu, From dual-aerogels with semi-interpenetrating polymer network structure to hierarchical porous carbons for advanced supercapacitor electrodes, *Colloids Surf. A Physicochem. Eng. Asp.* 649 (2022), 129356.
- [47] Z.B. Lei, L. Lu, X.S. Zhao, The electrocapacitive properties of graphene oxide reduced by urea, *Energy Environ. Sci.* 5 (2012) 6391–6399.
- [48] Y. Zhou, X. Ren, Y. Du, Y. Jiang, J. Wan, F. Ma, In-situ template cooperated with urea to construct pectin-derived hierarchical porous carbon with optimized pore structure for supercapacitor, *Electrochim. Acta* 355 (2020), 136801.
- [49] F.M. Hassan, V. Chabot, J. Li, B.K. Kim, L. Ricardez-Sandoval, A. Yu, Pyrrolic-structure enriched nitrogen doped graphene for highly efficient next generation supercapacitors, *J. Mater. Chem. 1* (2013) 2904–2912.
- [50] N.D. Kim, D.B. Buchholz, G. Casillas, M. José-Yacaman, R.P.H. Chang, Hierarchical design for fabricating cost-effective high performance supercapacitors, *Adv. Funct. Mater.* 24 (2014) 4186–4194.
- [51] B. Chen, X. Zhong, G. Zhou, N. Zhao, H.-M. Cheng, Graphene-supported atomically dispersed metals as bifunctional catalysts for next-generation batteries based on conversion reactions, *Adv. Mater.* 34 (2022), 2105812.
- [52] S. Kumar, G. Saeed, L. Zhu, K.N. Hui, N.H. Kim, J.H. Lee, 0D to 3D carbon-based networks combined with pseudocapacitive electrode material for high energy density supercapacitor: a review, *Chem. Eng. J.* 403 (2021), 126352.
- [53] Z. Li, S. Gadipelli, H. Li, C.A. Howard, D.J.L. Brett, P.R. Shearing, Z. Guo, I. P. Parkin, F. Li, Tuning the interlayer spacing of graphene laminate films for efficient pore utilization towards compact capacitive energy storage, *Nat. Energy* 5 (2020) 160–168.
- [54] S. Zhu, X. Sun, X. Gao, J. Wang, N. Zhao, J. Sha, Equivalent circuit model recognition of electrochemical impedance spectroscopy via machine learning, *J. Electroanal. Chem.* 855 (2019), 113627.
- [55] Y. Zhu, S. Murali, M.D. Stoller, K.J. Ganesh, W. Cai, P.J. Ferreira, A. Pirkle, R. M. Wallace, K.A. Cyrosz, M. Thommes, D. Su, E.A. Stach, R.S. Ruoff, Carbon-based supercapacitors produced by activation of graphene, *Science* 332 (2011) 1537–1541.
- [56] X. Deng, J. Li, S. Zhu, L. Ma, N. Zhao, Boosting the capacitive storage performance of MOF-derived carbon frameworks via structural modulation for supercapacitors, *Energy Storage Mater.* 23 (2019) 491–498.
- [57] P. Jiang, J. Chen, C. Wang, K. Yang, S. Gong, S. Liu, Z. Lin, M. Li, G. Xia, Y. Yang, J. Su, Q. Chen, Tuning the activity of carbon for electrocatalytic hydrogen evolution via an iridium-cobalt alloy core encapsulated in nitrogen-doped carbon cages, *Adv. Mater.* 30 (2018), 1705324.
- [58] S.-F. Hung, A. Xu, X. Wang, F. Li, S.-H. Hsu, Y. Li, J. Wicks, E.G. Cervantes, A. S. Rasouli, Y.C. Li, M. Luo, D.-H. Nam, N. Wang, T. Peng, Y. Yan, G. Lee, E. H. Sargent, A metal-supported single-atom catalytic site enables carbon dioxide hydrogenation, *Nat. Commun.* 13 (2022) 819.
- [59] J. Chen, Y. Huang, N.N. Zhang, H.Y. Zou, R.Y. Liu, C.Y. Tao, X. Fan, Z.L. Wang, Micro-cable structured textile for simultaneously harvesting solar and mechanical energy, *Nat. Energy* 1 (2016), 16138.
- [60] S. Afroj, S.R. Tan, A.M. Abdelkader, K.S. Novoselov, N. Karim, Highly conductive, scalable, and machine washable graphene-based E-textiles for multifunctional wearable electronic applications, *Adv. Funct. Mater.* 30 (2020), 2000293.
- [61] D. Li, L. Dai, X. Ren, F. Ji, Q. Sun, Y. Zhang, L. Ci, Foldable potassium-ion batteries enabled by free-standing and flexible SnS₂@C nanofibers, *Energy Environ. Sci.* 14 (2021) 424–436.
- [62] T. Ling, P. Da, X. Zheng, B. Ge, Z. Hu, M. Wu, X.-W. Du, W.-B. Hu, M. Jaroniec, S.-Z. Qiao, Atomic-level structure engineering of metal oxides for high-rate oxygen intercalation pseudocapacitance, *Sci. Adv.* 4 (2018) eaau6261.